Effect of High Pressure Torsion on Crystallization and Magnetic Properties of $Fe_{73.9}Cu_1Nb_3Si_{15.5}B_{6.6}$

Monika Antoni[a,*] , Florian Spieckermann[a] , Viktor Soprunyuk[b,e], Niraj Chawake[b] , Baran Sarac[b], Jakub Zálešák[b], Christian Polak[c], Christoph Gammer[b], Reinhard Pippan[b], Michael Zehetbauer[d], Jürgen Eckert[a,b]

a Department of Materials Science, Chair of Materials Physics, Montanuniversität Leoben, Leoben, Austria

b Erich Schmid Institute of Materials Science, Austrian Academy of Sciences, Leoben, Austria

c Vacuumschmelze GmbH & Co KG (VAC) Rapid Solidification Technology, Hanau, Germany

d Research Group Physics of Nanostructured Materials, Faculty of Physics, University of Vienna, Vienna, Austria

e Research Group Physics of Functional Materials, Faculty of Physics, University of Vienna, Vienna, Austria

Abstract

The effects of severe plastic deformation (SPD) by means of high pressure torsion (HPT) on the soft magnetic properties of the iron-based metallic glass $Fe_{73.9}Cu_1Nb_3Si_{15.5}B_{6.6}$ are investigated. With this procedure, it has been possible for the first time to consolidate and deform this high-strength material with a minimum of cracks. X-ray diffraction, differential mechanical and differential scanning analyses, as well as optical and scanning electron microscopy were carried out for characterization of crystallization phenomena and crack formation. For magnetic properties, minor loop hysteresis measurements were done because of their high sensitivity for magnetic structures. Significant influences of HPT-processing on the coercivity as well as on magnetic anisotropy are found and discussed in detail.

Introduction

$Fe_{73.9}Cu_1Nb_3Si_{15.5}B_{6.6}$ is a widely used industrial soft magnetic material with high saturation polarization. It is manufactured as an amorphous tape by melt spinning in air starting from a master alloy made from industrial grade pre-alloys. Subsequent annealing creates nanocrystals and affects their size while their orientation and magnetic anisotropy are controlled by annealing of the material either with an external magnetic field, or by plastic deformation [1], [2]. Yet, the latter has not been applied extensively because of the brittleness of amorphous material. Previous attempts [3], [4] to create bulk amorphous or amorphous/nanocrystalline samples were not successful so far. Also methods of severe plastic deformation ('SPD', e.g. [5], [6], [7], and [8]) were applied to very small samples only. Therefore, this work aimed to apply high pressure torsion (HPT) – the most efficient technique among all the severe plastic deformation SPD methods [9] – to obtain large amorphous samples, and to develop a feasible route to produce bulk crack-free samples. Such a technique would be very important for e.g. producing bulk-shape transformer cores with a minimum of magnetic losses.

Before and after application of HPT the samples were investigated with regard to their microstructural and crystallographic features on different length scales, with emphasis to the thermal properties of the amorphous precursor alloy. After HPT, also the magnetic properties of selected samples were measured and will be discussed especially with respect to the effect of HPT on coercivity and magnetic anisotropy.

Experimental

Amorphous $Fe_{73.9}Cu_1Nb_3Si_{15.5}B_{6.6}$ ribbons (VITROPERM) were fabricated by single-roller melt spinning and supplied by Vacuumschmelze GmbH, Hanau, Germany.

At first, thermomechanical analyses were performed on the amorphous tape material using differential scanning calorimetry (DSC), and dynamic mechanical analysis (DMA). The characteristic temperatures for the crystallization $T_{x,n}$ as well as their respective activation energies $E_{a,n}$ have been determined by DSC (Pegasus 404 F1, Netzsch). DMA methods (Discovery Hybrid Rheometer DHR 3 in tension mode, TA Instruments) were used to determine the glass transition temperature T_g, which was difficult to be exactly determined by DSC. Similar to the dielectric relaxation in polymers, we used a symmetric Cole-Cole function [10] for the description of the relaxation process in amorphous materials

$$Y^*(\omega) = Y_\infty + \frac{\Delta Y}{1+(i\omega\tau)^{1-\alpha}} \quad , \tag{1}$$

where Y^* is the complex elastic constant, ω is the angular frequency, α corresponds to the shape characteristics of the curve (taking a value between 0 and 1), and τ is the relaxation time that can be calculated as follows:

$$\tau = \tau_0 e^{\frac{E_a}{k_B T}} \quad . \tag{2}$$

Here, E_a is the activation energy, k_B the Boltzmann constant, and T the DMA peak temperature.

For the HPT experiments, a custom-made facility with 400 kN capacity, equipped with an induction heating system (TTH8, IEW Gumpoldskirchen, Austria) [11] was used. VITROPERM ribbons of 22 µm thickness were cut in squares of 12 x 12 mm² and stacked within the HPT anvils which had cavity of 8 mm diameter and 0.1 mm depth. The samples were torsionally deformed for one rotation each, at pressures between 4 and 7.5 GPa, and temperatures T = 473 – 673 K, see Table 1. The initial total thicknesses of the stacks before HPT-processing were between 500 µm and 1000 µm, while the final samples' thicknesses after HPT-processing varied between 425 and 750 µm (Tab. 1). The decrease of sample thickness arose from (i) the consolidation process of the ribbon, and (ii) compression before and during HPT. The torsional shear strain γ achieved by HPT was estimated by eq. (3)([9], for details on the validity of this equation, see [12]):

$$\gamma = \frac{2\pi N r}{t} \quad . \tag{3}$$

Here, N denotes the number of rotations, r the distance from the torsion axis (in our case, r = 3.5 mm as the site where the stripes perpendicular to the disc plane axis were cut for the subsequent magnetic measurements). For the estimations of γ given in Tab. 1, the final sample thicknesses t were used; their decrease during HPT was neglected because of the ambiguities (i, ii) mentioned above; therefore they represent upper limits of γ. Assuming an error in thickness measurements of about 10 µm, the errors of the estimated γ values given in Tab. 1 are about 1% - 5% for the thickest and the thinnest sample, respectively. HPT-processing was performed at elevated temperatures (T = 473 K, 573 K and 673 K) and two different pressures (p = 4 GPa, 7.5 GPa).

	p = 4 GPa		p = 7.5 GPa	
	t [μm]	γ	t [μm]	γ
T= 473 K	750	29.3	425	51.7
T= 573 K	550	40.0	573	38.4
T= 673 K	733	30,0	615	35.8

Tab. 1: Values of torsional shear strain γ calculated from the final thicknesses by means of eq. (3) for different HPT parameters p (pressure) and processing temperature (T).For errors of quantities t, γ, see text.

X-ray diffraction (XRD) measurements were performed using a benchtop XRD system with Co K_α anode and Fe K_β-filter (Bruker D2 Phaser). After the experiment, the background and $K_{\alpha 2}$ contribution were separated from the measured data. The as-quenched tape was investigated by diffraction experiments at the HEMS P07 beamline at PETRA III (DESY), Hamburg, Germany.

After being carefully cut in halves by a diamond wire saw, cross-sections of the HPT-processed samples were mechanically polished for optical light microscopy (Olympus BX 51 M) and scanning electron microscopy (LEO 1525, Zeiss) for investigations with emphasis on checking for cracks.

Magnetic properties were first investigated on tape-wound ring samples of the original VITROPERM ribbons using a custom-built hysteresograph as described in [13]. For the HPT-processed samples, another custom-constructed hysteresograph setup was used; in contrast to the other first one, this hysteresograph was operated by the solenoid method as described in [14], which was capable to measure small crack-free areas with dimensions 1.0 x 0.5 x 4.0 mm cut from the HPT-processed disks. In this case, a correction of the demagnetizing factor of the HPT-processed samples had to be done according to [15].

Results and Discussion

Differential thermal measurements of the amorphous state. For optimizing the HPT conditions, the thermal characteristics of the amorphous precursor alloy were investigated by DMA and DSC experiments. With DMA, the identification of the glass transition was possible getting a typical temperature of T_g = 740 ± 0.5 K (DMA 0.05 Hz) using a heating rate of 10 K/min. The corresponding activation energy was determined as $E_{a,g}$ = 282 ± 28 kJ/mol using the slope of the Arrhenius plot (eq. (2)) and T_g from the onset of the storage modulus drop (Fig. 1 (a)). DSC was carried out by heating from room temperature to 1273 K at heating rates between 5 and 50 K/min, in order to evaluate the temperatures T_{x1} and T_{x2} at the peak positions of the first and second stage of crystallization, respectively. For the heating rate of 10 K/min, this resulted in T_{x1} = 801± 5 K and T_{x2} = 967 ± 5 K (Fig. 1 (b)). Using the Kissinger method [16] the respective activation energies have been calculated as $E_{a,x1}$ = 472 ± 10 kJ/mol and $E_{a,x2}$ = 470 ±30 kJ/mol. The value of $E_{a,x1}$ for the first stage of crystallization is in good agreement with literature data of similar alloys [17], [18], [19], [20], [21], [22]; that of the second stage of crystallization is identical to the first one at least with regard to the measuring errors; we note that the theory of crystallization [23] suggests $E_{a,x2} > E_{a,x1}$ for $T_{x2} > T_{x1}$ rather than $E_{a,x2} < E_{a,x1}$ so that one must assess the measured values $E_{a,x1}$ and $E_{a,x2}$ as a lower limit for the true value of $E_{a,x2}$. When comparing our results with previous data obtained for a similar alloy, Gavrilovic et al. [24] have shown that the first stage of crystallization corresponds to the formation of the soft magnetic α-Fe-Si phase whereas at the second stage the development of hard magnetic iron borides like Fe_2B occurs. (see also [25]). The activation energy for this latter crystallization stage, however, has been measured for the first time in this paper.

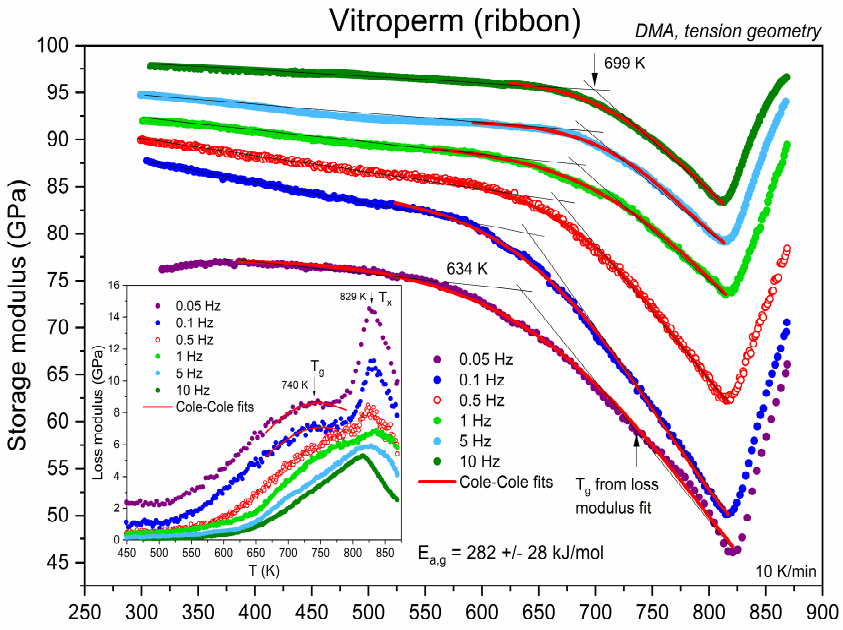

(a)

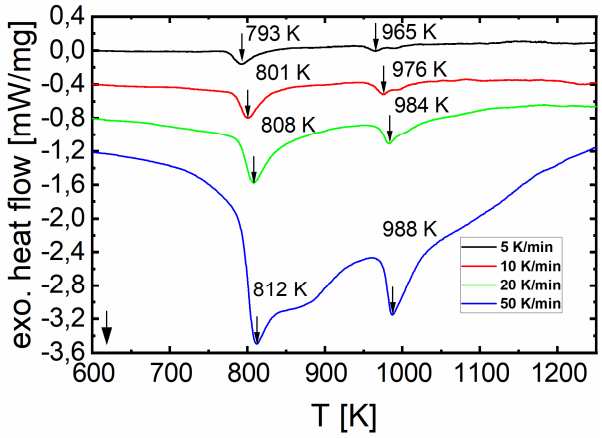

(b)

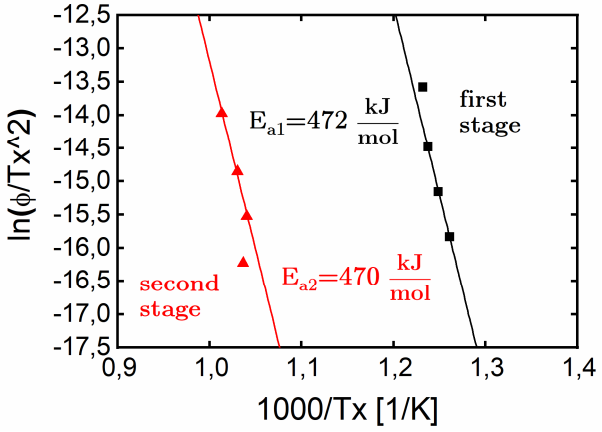

(c)

Fig. 1: Differential heating experiments showing the glass transition at T_g and its activation energy $E_{a,g}$ from DMA measurements recorded at different frequencies (a), the crystallization temperatures T_{x1} and T_{x2}, obtained from DSC scans at different heating rates (b), and their corresponding activation energies $E_{a,x1}$, $E_{a,x2}$ (c). For errors in the measured temperatures, see the text.

Microstructural investigations: XRD analyses. Prior to the HPT experiments, the microstructural properties were investigated. Fig 2 (a) shows the diffraction pattern of the $Fe_{73.9}Cu_1Nb_3Si_{15.5}B_{6.6}$ melt-spun ribbon, confirming the amorphous nature of the starting material. Fig 2 (b) and (c) show the XRD results after HPT. The patterns indicate a sharpening of the first amorphous diffraction maximum around q = 31 nm^{-1} as well as the appearance of satellite peaks left and right of both amorphous diffraction maxima. Those features might be related to the known occurrence of first nanograin nucleation processes as induced by Cu-rich clusters [25], [26]; and might be facilitated by increasing the HPT pressure and temperature. Moreover, the samples HPT-processed at 573 K and 673 K show the evolution of new small peaks around q = 44, 54 and 62 nm^{-1} (Fig 2 (b,c)) confirming the increasing formation of nanocrystals out of pure α-Fe (see also [25]). Those peaks get slightly more significant the higher the HPT temperature and the higher the hydrostatic pressure applied. An upper-limit estimation of the peak width by means of the Scherrer equation gives a maximum crystallite size of about 3 nm. Nevertheless, the overall volume fraction of the nanocrystalline grains seems to be in the order of a few percent in the amorphous matrix for all samples.

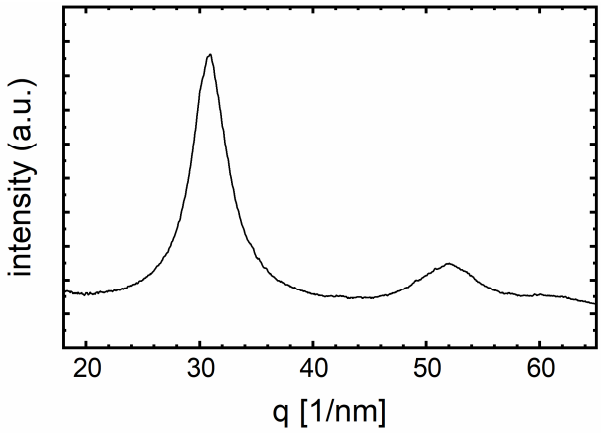

(a)

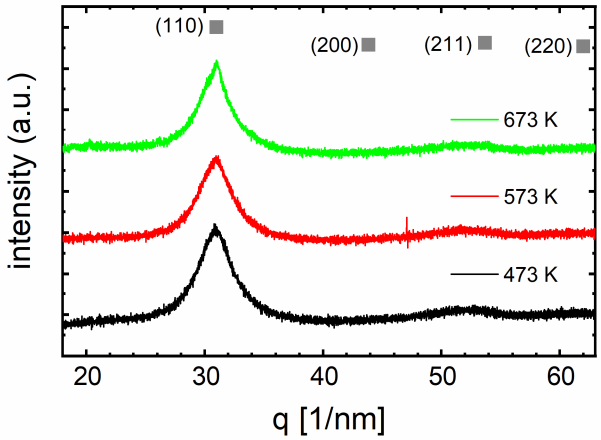

(b)

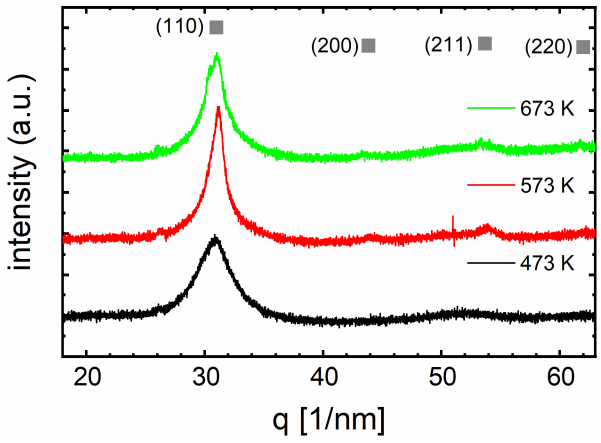

(c)

Fig. 2: Synchrotron diffraction experiments showing the amorphicity of the as-quenched melt-spun ribbon (a); XRD measurements after HPT-processing at two different pressures (b) 4 GPa and (c) 7.5 GPa, all at three different temperatures 473 K (black), 573 K (red) , and 673 K (green). In comparison with the as-quenched state (Fig. 2 (a)), some of the HPT-processed samples (Figs. 2 (b) and (c)) exhibit new peaks emerging at positions indicated by full squares (respective (hkl)-indices of α-Fe given).

Microstructural investigations: Optical microscopy. OM investigations of the polished cross-sections after HPT-processing have been undertaken for all differently deformed samples. The findings show that fewer cracks are present in the outer regions of the samples when HPT-processed at 473 K, 7.5 GPa (see Fig 3 (b)) and at 573 K, 7.5 GPa (see Fig 3 (d)). Further investigations by SEM (see Fig 4) confirm these results as they show only sparsely dispersed cracks of submicrometer width. These results are an important prerequisite for the reliability of subsequent magnetic measurements that should be done on crack-free specimens.

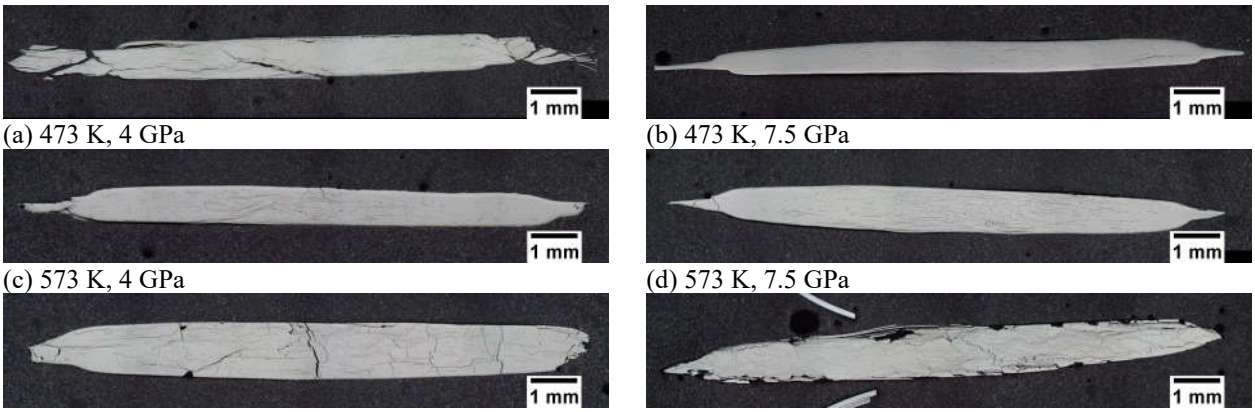

(a) 473 K, 4 GPa (b) 473 K, 7.5 GPa

(c) 573 K, 4 GPa (d) 573 K, 7.5 GPa

(e) 673 K, 4 GPa (f) 673 K, 7.5 GPa

Fig. 3: OM images of the polished cross-sections of the samples after HPT-processing for one rotation each. The most promising microstructures develop for conditions (b) and (d).

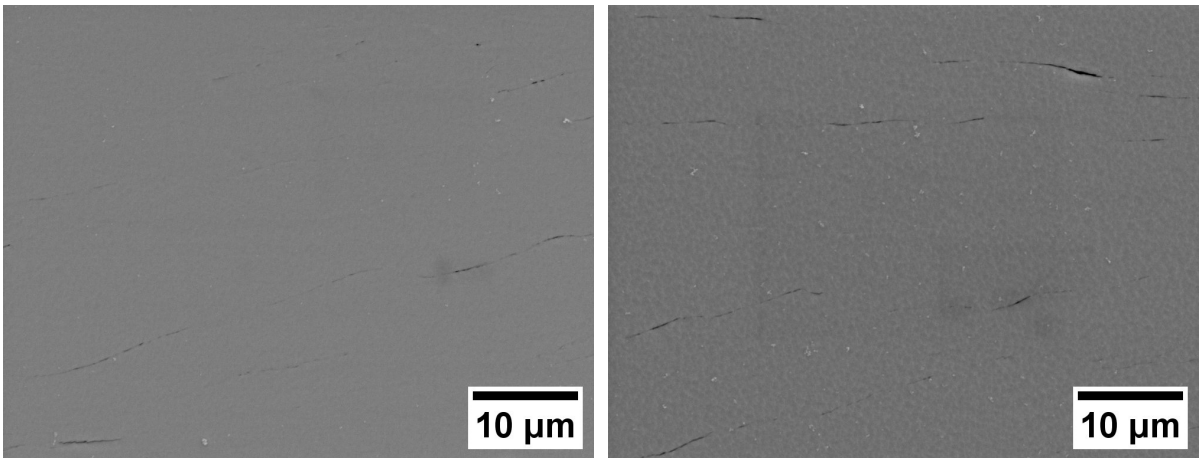

(a) 473 K, 7.5 GPa (b) 573 K, 7.5 GPa

Fig. 4: SEM images (SE detector) taken 3.5 mm from the center of selected HPT-samples.

Magnetic measurements. A tape-wound core was made from the as-cast melt spun ribbon to assess the magnetic properties of the amorphous material and its frequency dependence. The core had an iron-cross section A_{Fe} = 3.52 mm^2 and a mean magnetic path length l_m = 177.19 mm. The primary winding number was N_1 = 48 and the secondary winding number was N_2 = 8. Measurements were performed using a triangular H field with an amplitude H_{max} = 1 kA/m for frequencies f = 10 Hz to f = 200 Hz.

Fig. 5 (a) shows the classical R-shape hysteresis as it is expected for an amorphous material [27]. Furthermore, using the frequency dependent measurements of the coercivity H_c, these were extrapolated to a value of 12 A/m at f = 0 Hz (Fig. 5 (b)). The plots of the relative permeability also include the frequency dependence (Fig. 5 (c)).

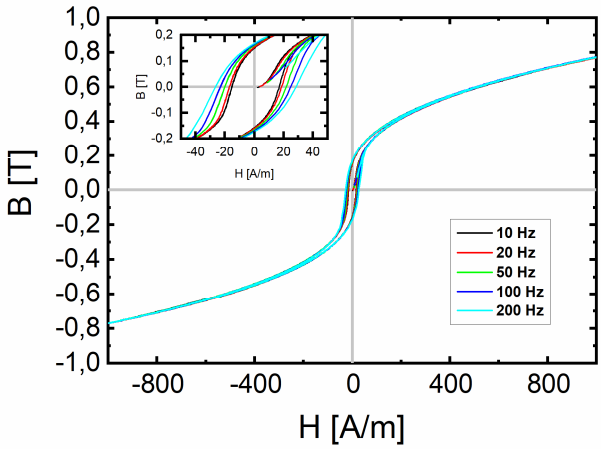

(a)

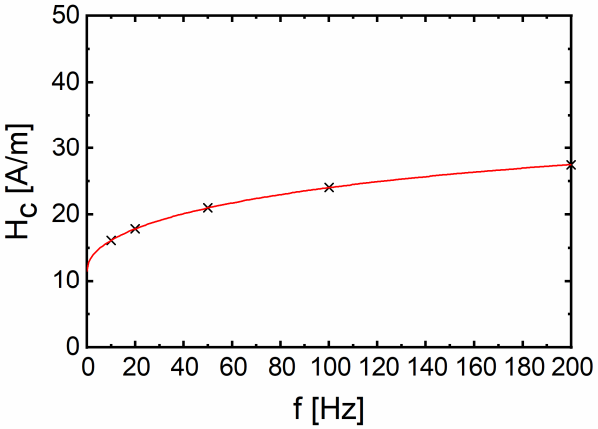

(b)

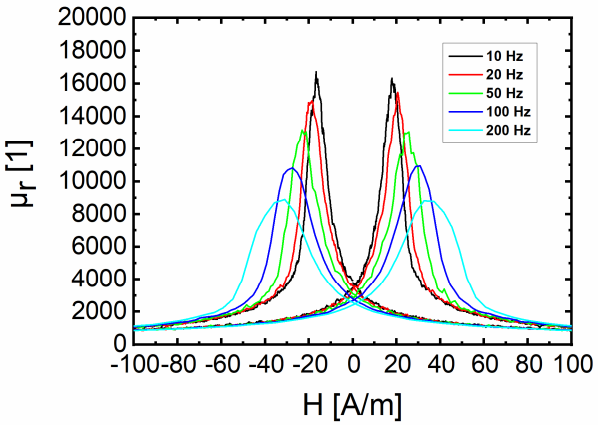

(c)

Fig. 5: Hysteresis data of tape-wound ring samples made from the amorphous tape showing the frequency dependence of the hysteresis (a), the coercivity H_c (b), as well as of the relative permeability μ_r (c).

The 'minor loop hysteresis' technique (which was carried out in a solenoid hysteresograph setup) was chosen to analyze the changes of the magnetic structure after applying HPT-processing to the initially amorphous samples. According to several papers (e.g. [28], [29], [30], [31]), minor loop hystereses can resolve very small differences in magnetic characteristics and/or microstructure. In particular, according to publications [2], [32] and [33], the slope of the hysteresis represents a measure for the magnetic anisotropy, irrespective of reaching saturation or not.

Fig. 6 (a) shows the minor loop characteristics obtained for a triangular H-field at 200 Hz (H_{max} = 700 A/m) in an amorphous tape-wound core, and compares it to the minor loop characteristics of two selected HPT-processed samples (Fig. 6 (b)). Air-flux compensated measurements were done at the same frequency and similar H-field amplitudes.

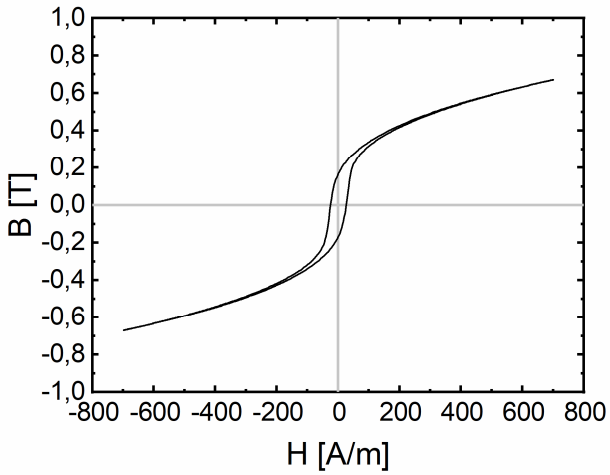

(a)

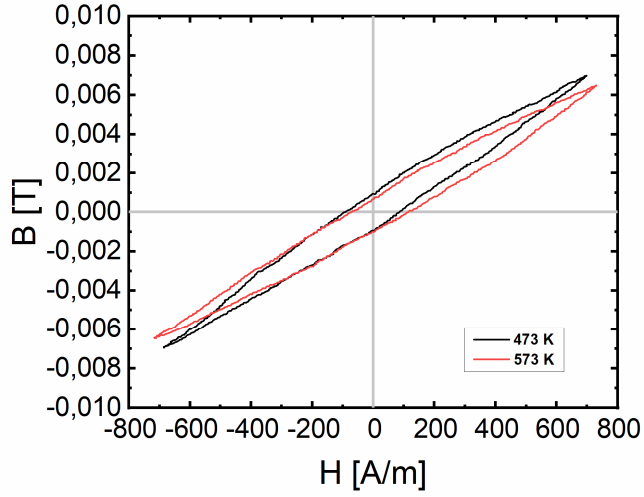

(b)

Fig. 6: Minor loop hystereses measured at f = 200 Hz showing the magnetic properties of a typical as-quenched sample (a) and of samples HPT-processed at 7.5 GPa at the indicated temperatures (b).

	H_c [A/m]	B_r [mT]	B_{max} [mT]	P/f [J/m^3]	<K> [J/m^3]
As-quenched (H_{max}=700 A/m)	25.4± 0.2	165.00± 2.0	671.0± 2.0	30.94± 0.4 *10^{-3}	123.05± 0.4 *10^{-3}
473 K, 7.5 GPa (γ = 51,7)	88.4± 5.4	0.94± 0.06	7.0± 0.06	1.58± 0.3 *10^{-3}	1.98± 0.3 *10^{-3}
573 K, 7.5 GPa (γ = 38,4)	91.8± 5.4	0.82± 0.06	6.5± 0.06	1.71± 0.3 *10^{-3}	1.96± 0.3 *10^{-3}

Tab. 2: Comparison of minor-loop hysteresis parameters at 200 Hz for as-quenched and selected HPT-processed samples.

Fig. 6 and Tab. 2 reflect the characteristic values of the minor loops: While H_c of the HPT-processed samples is significantly higher than that of the as-quenched ribbon (while the HPT-processing temperature as well as the deformation strain are less important), the remanence B_r is substantially smaller than in the undeformed sample, as is the amplitude of the B-field B_{max}. The anisotropy energy density <K> which is represented by the hysteresis area between the upper magnetization curve and the B-axis (see [34]), shows a significantly lower value in both HPT-processed states compared to that of the as-quenched state. This means, however, a significant decrease in the slope in the hysteresis curve so that the magnetic anisotropy in the HPT-processed samples must be much larger than in the as-quenched state. A similar – although much smaller – tendency is seen in comparing the B/H characteristics of the two HPT-processed samples (Fig. 6 (b)): that of the sample with the higher HPT-processing temperature is somewhat flatter, suggesting that this effect comes from first precursors of nanocrystallization as suggested by the XRD pattern of the HPT sample processed at higher temperature. This finding fits well to the steeper slope of the hysteresis of the sample being HPT-processed at 473 K with 7.5 GPa, indicating that the sample and/or its magnetic orientation is closer to the magnetic easy axis than the sample which was HPT-processed at 573 K with 7.5 GPa. At lower HPT-processing temperature as well as at higher shear strain, the crystal orientation distribution is more similar to textures typical of HPT-processing being more random and isotropic, which is in agreement with the findings of Aronin's [5] and Pippan's [35] group, both having applied HPT at lower temperature and up to much higher deformations. The experiments presented in [5], [6] and [7] also show an increase of H_c with increasing extent of HPT deformation.

The crystalline peaks seen in the XRD patterns (Figs. 2b and c) for the HPT-processed samples are close to the resolution limit of the measurements, which let us estimate the volume fraction of crystallites to be not larger than about 1 vol.%. Therefore, the crystalline fraction cannot significantly contribute to the observed HPT-induced increases of H_c.

Hernando [36] and Gonzales et al. [37] have extensively investigated the helical magnetic anisotropy in torsionally deformed amorphous soft magnetic metals. The occurrence of helical domains in the amorphous samples as a result of HPT could also lead to the Mateucci effect/invers Wiedemann effect with similar results of the anisotropy [36, 37]. However, in this work the samples were prepared and measured transversely to the torsional axis, in contrast to the investigations reported in [36, 37]. Thus, in the present study, the formation of helical domains is improbable, although a complex domain structure due to the HPT deformation induced stress state might be present.

It is well known that VITROPERM-type alloys have a large magnetostriction of $\lambda_S \sim 26$ ppm in the amorphous state as compared to their magnetostriction of ~ 0.2 ppm in the nanocrystalline state [25]. Because the coercivity is proportional to the product $\lambda_S.\sigma$ (where σ stands for the internal stress of the material), H_c depends more on σ the higher λ_S is. As indicated by Pershina et al. [5], the formation of shear bands accounts for an enormous increase of internal stresses, and indeed, with increasing HPT-induced shear deformation, a substantially high density of shear bands evolves [8]. This massive formation of shear bands can explain the observed flattening of hysteresis, as (at least compressive) stresses in a material with high λ_S are known to cause such flattening [38].

Summary and conclusions

The most important results presented in this paper are as follows:

- HPT is a feasible route to manufacture crack-free bulk samples from $Fe_{73.9}Cu_1Nb_3Si_{15.5}B_{6.6}$ melt-spun ribbons.

- For the first time, the activation energy $E_{a,g}$ of the glass transition in $Fe_{73.9}Cu_1Nb_3Si_{15.5}B_{6.6}$ was measured by DMA; it equals $E_{a,g}$ = 282 (±28) kJ/mol.

- The activation energy E_{a1} for the first stage of crystallization amounts to 472 ±10 kJ/mol which coincides well with literature values for similar alloys. The activation energy E_{a2} for the second stage of crystallization - which has not been measured so far in literature - is identical to that of the first stage within a measuring error of ± 30 kJ/mol, but in fact has to be larger because of the significantly higher crystallization temperature of the second stage.

- HPT-processing of the as-quenched amorphous alloy induced the formation of crystals but with a volume fraction of 1 vol.% at maximum, and crystallite with sizes ~ 3 nm at maximum. Therefore, the HPT-induced changes observed in the magnetic properties must come from structural changes of the amorphous phase which are most probably correlated with the deformation-induced formation of shear bands and the stress induced magnetic anisotropy.

- HPT induces a marked coercivity increase, a significant increase of magnetic anisotropy, as well as a decreased anisotropy energy density. These effects are caused by an increasing level of internal stresses, which seem to be connected with the occurrence of a large number of shear bands during HPT-processing.

In conclusion, processing by high pressure torsion (HPT) turned out to be a promising route to manufacture crack-free samples out of $Fe_{73.9}Cu_1Nb_3Si_{15.5}B_{6.6}$ ribbons. However, some need for improvement is left for the magnetic properties resulting from HPT treatment concerning the still rather high coercivity and low saturation polarization. With forthcoming experiments, the HPT parameters are

to be optimized with respect to a minimum of internal stresses as well as to a maximum of fraction of crystalline phase.

Acknowledgements

We would like to thank the European Research Council, Grant ERC-2013-ADG-340025 for support and cooperation. We acknowledge DESY (Hamburg, Germany) for the access to the High Energy Materials Science Beamline HEMS P07 at synchrotron PETRA III with all its experimental facilities, and Dr. Norbert Schell (HZG) for his kind assistance there.

References

[1] G. Herzer, S. Flohrer, C. Polak, IEEE Trans. Magn. 46 (2010) 341.

[2] G. Herzer, J. Magn. Magn. Mater. 133 (1994) 248.

[3] A. Inoue, B. Shen, Mater. Trans. 43 (2002) 766.

[4] A. Inoue, B. Shen, T. Ohsuna, Mater. Trans. 43 (2002) 2337.

[5] E. A. Pershina, G. E. Abrosimova, A. S. Aronin, D. V. Matveev, Phys. Solid State 57 (2015) 234.

[6] G. Abrosimova, A. Aronin, D. Matveev, E. Pershina, Mater. Lett. 97 (2013) 15.

[7] A. Aronin, G. Abrosimova, D. Matvev, O. Rybchenko, Rev. Adv. Mater. Sci. 25 (2010) 52.

[8] G. E. Abrosimova, A. S. Aronin, S. V. Dobatkin, I. I. Zver'kova, D. V. Matveev, O. G. Rybchenko, E. V. Tat'yanin, Phys. Solid State 49 (2007) 1034.

[9] R. Pippan, S. Scheriau, A. Hohenwarter, M. Hafok, Mater. Sci. Forum 584 (2008) 16.

[10] K. Menard, Dynamic Mechanical Analysis: A practical introduction, CRC Press, Boca Raton, FL, (2008)

[11] S. Scheriau, Z. Zhang, S. Kleber, R. Pippan, Mater. Sci. Eng., A 528 (2011) 2776.

[12] Y. Beygelzimer, R. Kulagin, L. S. Toth, Y. Ivanisenko, Beilstein J. Nanotech. 7 (2016) 1267.

[13] OVE EN 60404-6: 2017 07 01

[14] IEC 60404-15: 2012 09 01

[15] A. Aharoni, J. Appl. Phys. 83 (1998) 3432.

[16] H. E. Kissinger, Anal. Chem., 29 (1957) 1702.

[17] Y. H. Ding, M. J. Li, B. H. Yang, X. Ma, Appl. Mech. Mater. 117 (2011) 901.

[18] H. X. Li, J. E. Gao, Y. Wu, Z. B. Jiao, D. Ma, A. D. Stoica, X. L. Wang, Y. Ren, M. K. Miller, Z. P. Lu, Sci. Rep. 3 (2013).

[19] M. Stoica, S. Kumar, S. Roth, S. Ram, J. Eckert, G. Vaughan, A. R. Yavari, J. Alloys Compd. 483 (2009) 632.

[20] M. A. Willard, M. Daniil, in Handb. Magn. Mater. Elsevier, Amsterdam (2013) 173.

[21] N. A. Mara, A. V. Sergueeva, A. K. Mukherjee, Mater. Sci. Eng., A 374 (2004) 244.

[22] N. Chau, N. Q. Hoa, N. D. The, P. Q. Niem, J. Magn. Magn. Mater. 304 (2006) 179.

[23] G. Gottstein, Physical Foundations of Materials Science, Springer Berlin Heidelberg, (2004).

[24] A. Gavrilović, D. M. Minić, L. D. Rafailović, P. Angerer, J. Wosik, A. Maričić, D. M. Minić, , J. Alloys Compd. 504 (2010) 462.

[25] G. Herzer, in Handb. Magn. Mater. Elsevier, Amsterdam (1997) 415.

[26] M. Vázquez, P. Marin, H. A. Davies, A. O. Olofinjana, Appl. Phys. Lett., 64 (1994) 3184

[27] G. Herzer, in Encyc. Mater.: Sci. and Tech. Elsevier (2001) 149.

[28] S. Takahashi, S. Kobayashi, H. Kikuchi, Y. Kamada, K. Ara, IEEE Trans. Magn. 42 (2006) 3782.

[29] S. Takahashi, T. Ueda, L. Zhang, J. Phys. Soc. Jpn. 73 (2004) 239.

[30] S. Takahashi, L. Zhang, J. Phys. Soc. Jpn. 73 (2004) 1567.

[31] Y. N. Starodubtsev, V. A. Kataev, K. O. Bessonova, V. S. Tsepelev, J. Magn. Magn. Mater. 479 (2019) 19.

[32] G. Bertotti, Hysteresis in Magnetism, Elsevier, Amsterdam (1998)

[33] S. Flohrer, G. Herzer, J. Magn. Magn. Mater. 322 (2010) 1511.

[34] B. D. Cullity, C. D. Graham, Introduction to Magnetic Materials, John Wiley & Sons, Inc., Hoboken, NJ (2008).

[35] S. Scheriau, M. Kriegisch, S. Kleber, N. Mehboob, R. Grössinger, R. Pippan, J. Magn. Magn. Mater. 322 (2010) 2984.

[36] A. Hernando, J. M. Barandiarán, Phys. Rev. B, 22 (1980) 2445

[37] J. Gonzalez, J. M. Blanco, J. M. Barandiaran, M. Vazquez, A. Hernando, G. Rivero, D. Niarchos, IEEE Trans. Magn., 26 (1990) 1798

[38] B. Bergmair, T. Huber, F. Bruckner, C. Vogler, M. Fuger, D. Suess, J. Appl. Phys. 115 (2014) 023905.